A Hankelization-Based Neural Network-Assisted Signal Classification in Integrated Sensing and Communication Systems

Zhang, Linyi; Ozger, Mustafa; Lee, Woong-Hee

Published in:
IEEE Access

DOI (link to publication from Publisher):
10.1109/ACCESS.2025.3574848

Publication date:
2025

Document Version
Publisher's PDF, also known as Version of record

IEEE Access
Multidisciplinary | Rapid Review | Open Access Journal

Received 21 April 2025, accepted 20 May 2025, date of publication 29 May 2025, date of current version 5 June 2025.

Digital Object Identifier 10.1109/ACCESS.2025.3574848

RESEARCH ARTICLE

A Hankelization-Based Neural Network-Assisted Signal Classification in Integrated Sensing and Communication Systems

LINYI ZHANG[1], MUSTAFA OZGER[1,2], AND WOONG-HEE LEE[3], (Member, IEEE)

[1]School of Electrical Engineering and Computer Science, KTH Royal Institute of Technology, 164 40 Stockholm, Sweden
[2]Department of Electronic Systems, Aalborg University, 2450 Copenhagen, Denmark
[3]Division of Electronics and Electrical Engineering, Dongguk University-Seoul, Seoul 04620, South Korea

Corresponding author: Woong-Hee Lee (woongheelee@dongguk.edu)

This work was supported in part by the Institute of Information & Communications Technology Planning & Evaluation (IITP) grant funded by Korean Government (MSIT) (Development of integrated interference analysis technology for improving frequency utilization efficiency) under Grant RS-2023-00217885, and in part by the Dongguk University Research Fund of 2024 under Grant S-2024-G0001-00025.

ABSTRACT In this paper, we introduce a neural network (NN)-based framework aimed at classifying sensing and communication signals at base stations, improving the efficiency of integrated sensing and communication (ISAC) systems in a bistatic configuration. The framework leverages a key mathematical insight: the Hankelized matrix formed from an equidistantly sampled signal of sparsely superimposed radio waves exhibits a low-rank property, whereas a frequency-modulated signal lacks this characteristic. It ensures that, even in practical environments, the Hankelized matrix of a sensing or communication channel statistically retains the relevant information. Hence, we use the singular values of the Hankelized matrix as the input to the neural NN, while the output is a one-hot encoded vector indicating whether the received signal is intended for sensing or communication. We investigate three scenarios where the communication and sensing signals either use the same or different waveforms in terms of the detection performance of the communication signals. The results demonstrate that the proposed method outperforms existing approaches in classification performance across all scenarios, regardless of whether the communication and sensing signals utilize the same waveform or not. The framework achieves a detection rate of over 95% even at an SNR of 0 dB. Notably, the network performs well in terms of a small number of pilot symbols, a small number of training dataset, and dynamic environments.

INDEX TERMS Integrated sensing and communication, neural networks, binary classification, Hankelization.

I. INTRODUCTION

Sensing technology plays an increasingly important role in future sixth-generation (6G) wireless networks, especially in emerging applications such as smart home [1], smart city [2], and various other services [3]. These applications necessitate not only high-performance wireless communication services but also high-accuracy sensing capabilities [4]. However, the traditional approach of independently designing communication and sensing systems often results in inefficient allocation of spectrum resources, exacerbating spectrum congestion issues. Fortunately, advancements in wireless technology, including the widespread adoption of massive multiple-input multiple-output (MIMO) technology [5] and the migration of wireless communication systems to higher frequency bands such as millimeter wave (mmWave) and terahertz (THz) bands [6], are blurring the boundaries between sensing and communication systems. Integrated sensing and communication is considered a promising technology for next-generation wireless networks and has received extensive attention from both industry and academia [7].

ISAC system is a unified system providing wireless communication and radar sensing functions [8]. Traditionally, sensing and communication have been treated separately, each with distinct requirements, protocols, and

The associate editor coordinating the review of this manuscript and approving it for publication was Barbara Masini.

hardware. However, the increasing demand for efficient spectrum use and the rise of applications such as Internet of Things (IoT) and intelligent transportation systems have sparked interest in integrating sensing into communication systems.

The ISAC system in 6G can deliver both device-based and device-free localization services, making it suitable for use cases that demand precise positioning, such as automated drone docking and coordinated robotic tasks. Moreover, the sensing capabilities of 6G, which support simultaneous imaging, mapping, and localization, enhance the performance of these functions collectively. This advancement paves the way for new possibilities in 3D imaging and mapping, both indoors and outdoors, even in non-line-of-sight scenarios [9].

Fig. 1 illustrates an ISAC scenario in a bistatic configuration, where the base station (BS) of interest receives communication signals from a user device and sensing signals, transmitted by a different BS, reflected off a sensing target. Enabling these capabilities may lead to the coexistence of different signals within the same baseband, as shown in Fig. 1, which will become more severe as wireless networks become more complex. In addition, developing a coordinated multi-point ISAC (CoMP-ISAC) system is an inevitable trend [10]. Managing signal transmission and processing sensing data across a wide area introduces complex cross-link interference (CLI) between multiple base stations (BS) [11]. A critical challenge lies in distinguishing between interference originating from the sensing component and that from the communication component [12]. Without precise interference identification, ISAC systems face heightened susceptibility to interference, which can impair communication quality, degrade sensing accuracy, and ultimately compromise system reliability [13]. To reduce the signaling overhead according to various protocols in upper layers and to better perform the sensing and communication tasks [4], it is necessary to differentiate between sensing and communication signals through simple operations using only the baseband signal.

Among different waveforms for sensing and communication in ISAC systems, frequency-modulated continuous-wave (FMCW) and orthogonal frequency division multiplexing (OFDM) are the most widely used [3]. FMCW is a well-designed waveform for various radar applications, including automotive, aerospace, and industrial sensing. FMCW radar transmits a continuous frequency-modulated signal [14], providing both range and velocity information simultaneously. In contrast, OFDM is a pivotal modulation technique in wireless communication systems [15]. It efficiently addresses high-speed data transmission challenges over wireless channels by segmenting the spectrum into multiple subcarriers. Furthermore, the OFDM signal is also used in combination with the linear frequency modulation (LFM), which is known as the OFDM-LFM signal [16]. It effectively improves the Doppler sensitivity and reduces the estimation error of velocity [17].

Existing ISAC signal processing methods focus on transmitter side design, i.e., ISAC beamforming and waveform design [3], [18]. However, the literature dealing with the received signal processing of ISAC systems is limited [19]. Distinguishing between communication and sensing signals received by a BS presents a significant challenge due to their similar distributions, which complicates classification using naive NN techniques. Some works such as [20], [21] focus on the problem of classifying modulation types in OFDM systems. In [22], the authors utilize a convolutional neural network (CNN) trained by in-phase and quadrature-phase (IQ) data from the received signal to classify whether the transmission scheme used in the transmitter is a single-carrier signal or an OFDM signal. However, single-carrier signals are less likely to be used in ISAC and the CNN used in the paper is large, making it less suitable for IoT applications.

In this paper, we present a new technique based on NNs for classifying sensing and communication signals based on the mathematical fact that the rank of the Hankelized matrix of an equidistant sampled radio signal is equal to the number of constituted radio waves. Previous studies have explored structural sparsity through Hankelization, applying it to detect the number of signals under sparse observations [23], to identify near and far field radiations [24], and to classify Rician and Rayleigh fading channels [25]. Building on this, our work utilize this property, offering new possibilities for classifying received signals in sensing and communication tasks. Our proposed method introduces a novel and compact NN framework that leverages channel information through Hankelization and singular value extraction, which is the first attempt to our knowledge. Our proposed problem and solution can be more effectively utilized in ISAC systems that share both sites and spectrum. For example, autonomous vehicles require simultaneous communication with other vehicles and infrastructure and sensing to detect obstacles and gather environmental data. Similarly, in smart homes or industrial IoT, devices must sense the environment and transmit data. Applying Hankelization and machine learning to distinguish communication signals from sensing signals can enable smarter resource scheduling and task identification. The contributions of the paper are outlined as follows:

- We formulate a classification problem to distinguish whether received signals are intended for sensing or communication tasks.
- We propose a novel NN-based classification framework that integrates signal processing techniques with the Hankel matrix representation of the received signal.
- We conduct comprehensive simulation studies to assess detection rate performance across various system parameters, including the number of training datasets and pilot symbols.
- We explore detection performance using diverse waveforms for sensing and communication signals.

The remainder of the paper is organized as follows. Section II provides detailed information on the system model and

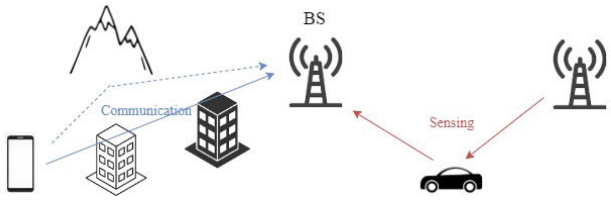

FIGURE 1. An ISAC scenario.

formulated the research problem. Section III explains the proposed method in detail. Section IV presents the extensive simulation studies. Finally, Section V concludes our paper.

II. SYSTEM MODEL AND PROBLEM FORMULATION

This section introduces our system model and problem formulation. Accordingly, we outline the key parameters and their respective definitions as follows:

- L: the number of multipaths.
- α_l: the complex channel gain of the l-th path.
- τ_l: the excess delay of the l-th path.
- v_l: the Doppler shift of the l-th path.
- f_0: the starting frequency of FMCW and OFDM signals.
- A_{sen}: the transmit signal amplitude for FMCW signal.
- κ: the chirp rate of the FMCW signal.
- Δf: the subcarrier spacing of the OFDM signal.
- P: the number of pilot symbols of the OFDM signal.
- K: the index spacing of the pilot assignment for the OFDM signal.

The channel impulse response (CIR) is written by the sum of Dirac-delta functions as follows:

$$h(\tau) = \sum_{l=1}^{L} \alpha_l \delta(\tau - \tau_l) e^{-j2\pi v_l \tau}. \tag{1}$$

In our system model, the transmitted signal can be either a sensing signal or a communication signal. We use the subscripts *sen* and *com* to distinguish sensing signals and communication signals, which are designed using FMCW and OFDM, respectively.

First, over the sensing duration T, the time-domain FMCW signal is given by:

$$x_{sen}(t) = A_{sen} e^{j2\pi \left(f_0 t + \frac{\kappa}{2} t^2\right)}, \quad 0 \le t < T, \tag{2}$$

where A_{sen} is the signal amplitude, f_0 is the starting frequency, and κ represents the linear frequency modulation rate of the FMCW signal. The received FMCW signal experiencing the multipath channel can be represented as follows:

$$y_{sen}(t) = \sum_{l=1}^{L} \alpha_l e^{j2\pi v_l t} x_{sen}(t - \tau_l) + n(t), \tag{3}$$

where $n(t)$ is additive white Gaussian noise (AWGN). Substituting the expression for $x_{sen}(t-\tau_l)$, the received signal becomes:

$$y_{sen}(t) = \sum_{l=1}^{L} \alpha_l e^{j2\pi v_l t} A_{sen} e^{j2\pi \left(f_0 (t-\tau_l) + \frac{\kappa}{2}(t-\tau_l)^2\right)} + n(t). \tag{4}$$

After down-conversion to baseband and applying an N-point FFT, the frequency-domain representation of the FMCW signal can be represented as follows:

$$\mathbf{y}_{sen}[n] = \sum_{k=0}^{N-1} \left(\sum_{l=1}^{L} \alpha_l e^{j2\pi v_l k T_s} \cdot A_{sen} e^{j2\pi \left(f_0 (kT_s - \tau_l) + \frac{\kappa}{2}(kT_s - \tau_l)^2\right)} \right) e^{-j2\pi \frac{nk}{N}} + \mathbf{n}[n], \tag{5}$$

where T_s is the sampling interval.

Next, the transmitted OFDM signal is represented in the time domain as follows:

$$x_{com}(t) = \sum_{n=0}^{N-1} \mathbf{d}[n] e^{j2\pi (f_0 + n\Delta f)t}, \quad 0 \le t < T, \tag{6}$$

where $\mathbf{d}[n]$ is the n-th subcarrier data symbol, Δf is the subcarrier spacing, and T is the OFDM symbol duration. After propagating through the multipath channel, the received OFDM signal can be represented as follows:

$$y_{com}(t) = \sum_{l=1}^{L} \alpha_l e^{j2\pi v_l t} x_{com}(t - \tau_l) + n(t). \tag{7}$$

Substituting the expression for $x_{com}(t-\tau_l)$, the received signal becomes:

$$y_{com}(t) = \sum_{l=1}^{L} \alpha_l e^{j2\pi v_l t} \sum_{n=0}^{N-1} \mathbf{d}[n] e^{j2\pi (f_0 + n\Delta f)(t-\tau_l)} + n(t). \tag{8}$$

In the frequency domain, after down-conversion and applying FFT, the received OFDM signal is expressed as:

$$\mathbf{y}_{com}[n] = \sum_{l=1}^{L} \alpha_l e^{-j2\pi n \Delta f \tau_l} e^{j2\pi v_l T} \mathbf{d}[n] + \mathbf{n}_{com}[n], \tag{9}$$

where $\mathbf{n}_{com}[n]$ represents noise in the frequency domain.

To focus on specific subcarriers,[1] we consider indices pK ($p = 0, 1, \ldots, P-1$), corresponding to a subset of the N-point FFT outputs. For the FMCW signal, the frequency-domain representation at these subcarriers is given by:

$$\mathbf{y}_{sen}[pK] = \sum_{k=0}^{N-1} \left(\sum_{l=1}^{L} \alpha_l e^{j2\pi v_l k T_s} \cdot A_{sen} e^{j2\pi \left(f_0 (kT_s - \tau_l) + \frac{\kappa}{2}(kT_s - \tau_l)^2\right)} \right) e^{-j2\pi \frac{pKk}{N}} + \mathbf{n}[pK]. \tag{10}$$

[1] Our study focuses on classifying the purpose of the received signal in an ISAC system into sensing and communication. Since the receiver has no prior information, it is obvious to achieve this by capturing values corresponding to pre-assigned pilot symbol subcarrier indices.

Similarly, the OFDM signal at the pK-th subcarriers is expressed as:

$$\mathbf{y}_{com}[pK] = \sum_{l=1}^{L} \alpha_l e^{-j2\pi pK\Delta f \tau_l} e^{j2\pi \nu_l T} d[pK] + \mathbf{n}[pK], \tag{11}$$

where $d[pK]$ is the pilot symbol at subcarrier pK.

Denoting the received signal with no prior information as $\mathbf{y}$, the objective is to design a *filter* f that maximizes the probability of correctly determining whether x_{sen} or x_{com} was transmitted. This can be formulated as a binary hypothesis testing problem, where we define:

$$\mathcal{H}_{\text{sen}} : x_{\text{sen}} \text{ was transmitted.}; \ \mathcal{H}_{\text{com}} : x_{\text{com}} \text{ was transmitted.} \tag{12}$$

The goal is to find a *filter* $f : \mathbf{y} \mapsto \{x_{sen}, x_{com}\}$ that maximizes the probability of correct classification as follows:

$$f^* = \arg\max_f \left[Pr(f(\mathbf{y}) = \mathcal{H}_{\text{sen}} | \mathbf{y}; \mathcal{H}_{\text{sen}}) + Pr(f(\mathbf{y}) = \mathcal{H}_{\text{com}} | \mathbf{y}; \mathcal{H}_{\text{com}}) \right]. \tag{13}$$

III. THE PROPOSED METHOD

A. LOW RANK PROPERTY OF THE HANKELIZED CHANNEL

Through the pilot symbols, let $\mathbf{h}_p$ denote partially estimated channel and all transmitted pilot symbols are β. $\mathbf{h}_p$ can be obtained by $\mathbf{h}_p = \mathbf{y}[pK]/\beta$ for all $p \in \{0, \ldots, P-1\}$.

The key idea of this study is whether $\mathbf{h}_p$ exhibits structural sparsity determined by the number of multipaths L. If the received signal $\mathbf{y}$ is composed of x_{com}, then $\mathbf{h}_p$ will naturally satisfy this condition. In contrast, if $\mathbf{y}$ is composed of x_{sen} $\mathbf{h}_p$ will inherently possess a higher degree of freedom due to the residual components of the FMCW signal. Therefore, it is crucial to process the extracted $\mathbf{h}_p$ to observe its structural sparsity. To achieve this, we utilize the low rank property of a newly structured matrix obtained through Hankelization.

Now, the Hankelized matrix for the partially estimated channel $\mathbf{H}$ is as follows:

$$\mathbf{H}[i,j] = \mathbf{h}_p[i+j]_{0\le i\le P_T-1, 0\le j\le P'_T-1}, \tag{14}$$

where P_T and P'_T are the row and column dimensions of $\mathbf{H}$, respectively. We set $\mathbf{H}$ as square as possible to extract the maximum number of singular values. Thus, if P is an even number, then $\mathbf{H}$ will be the matrix that $P'_T = P_T + 1$; otherwise, $\mathbf{H}$ will be the square matrix ($P_T = P'_T$).

To discuss the usefulness of Hankelization, let $\mathbf{H}^*$ be the noise-free $\mathbf{H}$ extracted from the partially captured channel. Assuming P_T is larger than the number of multipaths L, we can find a useful property regarding the low rank of $\mathbf{H}^*$ as follows:

$$\text{rank}(\lim_{\gamma_{\text{SNR}}\to\infty} \mathbf{H}) = \text{rank}(\mathbf{H}^*) = L, \tag{15}$$

where γ_{SNR} is signal-to-noise ratio (SNR) in a channel. Since A_{sen} does not affect the analysis of structural sparsity, it is set to 1. To validate (15), let us take a closer look at an arbitrary row of $\mathbf{H}^*$, denoted by $\mathbf{H}^*[n,:]$, where $n \in \{0, 1, \ldots, P_T-1\}$. This is represented as follows:

$$\mathbf{H}^*[n,:] = \{\sum_{l=1}^{L} a_l e^{-j2\pi K(p+n)(\Delta f \tau_l + \nu_l T)}\}_{p=0}^{P_T-1}. \tag{16}$$

As shown above, $\mathbf{H}^*[n,:]$ is a linear combination of L number of P'_T-sized row vectors which are captured from the l-th multipath component of channel frequency response $\mathbf{h}$ which is the FFT result of $h(\tau)$. For simplicity, we denote this l-th multipath component of $\mathbf{h}$ in $\mathbf{H}^*[n,:]$ as $\mathbf{h}_l[n]$. Naturally, $\mathbf{H}^*[n,:] = \sum_{l=1}^{L} \mathbf{h}_l[n]$. Then, we can easily verify (15) while checking that all rows in $\mathbf{H}^*[n,:]$ have different L bases. Firstly, two row vectors of $\mathbf{h}_l[n]$ and $\mathbf{h}_l[m]$ are linearly dependent where $n, m \in \{0, 1, \ldots, P_T-1\}$, and $n \neq m$. This is because $\mathbf{h}_l[n]$ can be represented as:

$$\mathbf{h}_l[n] = e^{-j2\pi K(n-m)(\Delta f \tau_l + \nu_l T)} \mathbf{h}_l[m], \tag{17}$$

i.e., $\mathbf{h}_l[n]$ is a constant multiple of $\mathbf{h}_l[m]$, and vice versa. Additionally, two row vectors of $\mathbf{h}_l[n]$ and $\mathbf{h}_{l'}[n]$ are linearly independent where $l, l' \in \{1, \ldots, L\}$ and $l \neq l'$. Thus, (15) is satisfied.

B. A NUMERICAL PROOF THROUGH DISSIMILARITY VISUALIZATION

To demonstrate that our method improves the discriminativeness of the given dataset, we will justify the use of Hankel matrix singular values through numerical analysis. Fig. 2 shows (a) the histogram of the original channel, (b) the FFT processed channel, and (c) the singular values of the Hankelized matrices in terms of channel magnitude and channel phase of OFDM and FMCW signals. The lower subfigure of Fig. 2(c) is a separate plot of only two of the singular values that are dominant. The difference between the original channel as well as the amplitude of the FFT channel is relatively small, while the difference between the FFT phase as well as the Hankelized matrices is more pronounced. This difference explains why classification using the phase of the signal processed by the FFT and the singular values of the partially captured channel Hankelized matrix is more effective compared to other methods. Therefore, rather than analyzing the received signal in the time or frequency domain to identify its purpose, interpreting the signal using our proposed method can further enhance its distinguishability.

C. DESIGN OF THE PROPOSED NN FRAMEWORK

We propose a harmonized design with Hankelization and NN utilization to seek the low-dimensional space to represent the complex channel data. Accordingly, we will define the required terms as follows:

- $\bar{\sigma} \in \mathbb{R}_+^{P_T}$: the vector of singular values of the Hankelized channel $\mathbf{H}$, which is sorted in descending order.
- $\mathbf{z} \in \{[1\ 0]^T, [0\ 1]^T\}$: the one-hot encoding vector representing communication or sensing signal, where $(\cdot)^T$ is the transpose operator.

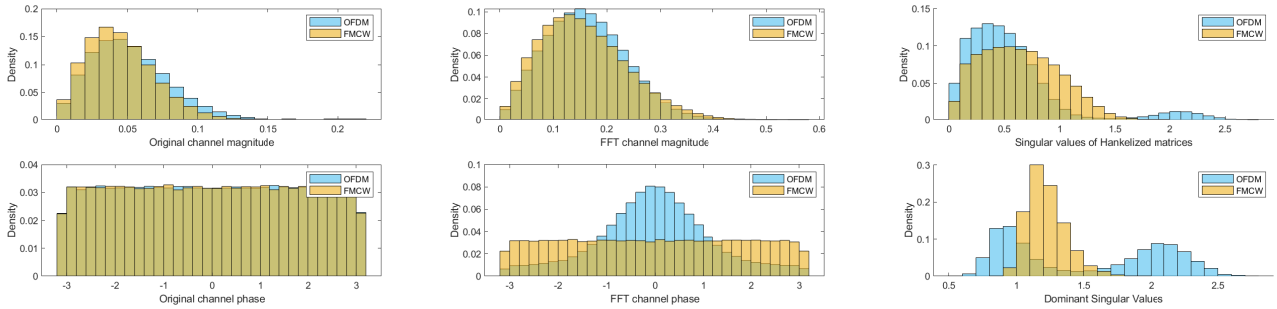

(a) Original channel (b) FFT-processed channel (c) Singular values of Hankelized matrices

FIGURE 2. **Histograms of utilizable data to classify ISAC signals.**

- S: the activation function for NNs; at the propagation between final hidden layer and the output layer, $S(a) = a$, i.e., the identity function; at other propagations between the adjacent layers, $S(a) = \frac{e^a - e^{-a}}{e^a + e^{-a}}$, i.e., the hyperbolic tangent function. $S(a) = (S(a[1]), \ldots, S(a[P_T]))^T$ where $a \in \mathbb{R}^{P_T}$ is an arbitrary input vector.
- Θ: the model parameters consisting of weight matrices and bias vectors.
- $\mathcal{N}_\Theta$: the NN model with the model parameters Θ.
- ∇_Θ: the gradient operator with respect to Θ.
- η: the learning rate related to the step size to update Θ.
- M: the total number of training dataset.

With above terms, we can define the optimized NN model, denoted by $\mathcal{N}_\Theta^*$, as follows:

$$\mathcal{N}_\Theta^* = \arg\min_{\mathcal{N}_\Theta} \frac{1}{M} \sum_{i=1}^{M} \|\mathbf{z}^{(i)} - \mathcal{N}_\Theta(\bar{\sigma}^{(i)})\|_2^2, \tag{18}$$

where i is the index of the training dataset. We set the mean squared error (MSE) as a loss function due to its simplicity and computational efficiency. In addition, we choose the stochastic gradient descent (SGD) as an optimizer. Hence, the update rule for the model parameter $\Theta^{(t)}$ at iteration t is

$$\Theta^{(t+1)} = \Theta^{(t)} - \eta \sum_{i \in B_t} \nabla_\Theta \left(\frac{1}{|B_t|} \sum_{i=1}^{|B_t|} ||\mathbf{z}^{(i)} - \mathcal{N}_\Theta(\bar{\sigma}^{(i)})||_2^2 \right), \tag{19}$$

where B_t are the current mini-batch.

Through the procedures of (18) and (19), we can optimize the fully connected NN (FC-NN) model. Now, we can use the optimized NN model for the hypothesis testing of binary classification as follows:

$$\hat{\mathbf{z}}[0] \underset{\text{sensing}}{\overset{\text{communication}}{\gtrless}} \hat{\mathbf{z}}[1], \text{ where } \hat{\mathbf{z}} = \mathcal{N}_\Theta(\bar{\sigma}). \tag{20}$$

Algorithm 1 shows the procedure of the proposed method.

Algorithm 1 The Procedure of Proposed NN-Based Framework

1: **[Training phase]**
2: Collect the training dataset, i.e., the captured channel $\mathbf{h}_p^{(i)}$ and the one-hot encoding vector $\mathbf{z}^{(i)}$ for all $i \in \{1, \ldots, M\}$.
3: **for** $i \leftarrow 1$**to**M **do**
4: Transform $\mathbf{h}_p^{(i)}$ to $\mathbf{H}^{(i)}$.
5: Extract the vector consisting of singular values of $\mathbf{H}^{(i)}$ in the descending order, i.e., $\bar{\sigma}^{(i)}$.
6: **end for**
7: Optimize the NN model based on (18) and (19), i.e., $\mathcal{N}_\Theta$, by inputting and outputting $\{\bar{\sigma}^{(1)}, \ldots, \bar{\sigma}^{(M)}\}$ and $\{\mathbf{z}^{(1)}, \ldots, \mathbf{z}^{(M)}\}$, respectively.
8: **[Test phase]**
9: Collect the test dataset, i.e., the captured channel $\mathbf{h}_p^{(j)}$ and the one-hot encoding vector $\mathbf{z}^{(j)}$ for all $j \in \{1, \ldots, M'\}$.
10: **for** $j \leftarrow 1$**to**M' **do**
11: Make the input vector $\bar{\sigma}^{(j)}$ referring steps 4 and 5.
12: Guess whether $\mathbf{h}_p^{(j)}$ is sensing or communication signal.
13: **end for**

TABLE 1. **Default configuration in the experiments.**

# pilot symbols	32	# training dataset	10^4
Carrier frequency	30 GHz	# test dataset	10^4
# multipaths	Uniform $[1, 8]$	Mini-batch size	8
NN connection type	FC-NN	Learning rate	10^{-5}
Loss function	MSE	Max. epochs	10^2
Optimizer	SGD	NN depth/width	2/16
SNR	10 dB	Path delay	Uniform
K-factor	3 dB	Max. excess delay	1μ sec
Small-scale fading	Jakes	Max. Doppler shift	5000 Hz

IV. SIMULATION RESULTS

This section compares the performance of our proposed NN-based scheme with a deep learning model using the original and FFT processed channels. The default settings and NN parameters for simulations are listed in Table 1.

In our analysis, we investigate the detection rate performance of the proposed method in relation to several factors: SNR, the size of the training dataset, the number of pilot symbols, SNR variations during the test phase. Subsequently, to analyze the scenario where both signals coexist, we examined the detection rate as a function of SIR. The signal-to-interference ratio (SIR) measures the quality of the communication signal while treating the sensing signal as interference.

We consider two scenarios: one where different waveforms are used for sensing and communication signals, specifically FMCW for sensing and OFDM for communication, and another where the same waveform, i.e., OFDM-LFM, is utilized for both objectives.

To the best of our knowledge this is the first trial to resolve a classification problem in ISAC systems. To verify whether our curated dataset from the proposed method is suitable for NN models, we utilized four transformations (i.e., magnitude extraction, phase extraction, magnitude extraction after FFT processing, and phase extraction after FFT processing) of the estimated channel $\mathbf{h}_p$ as inputs while maintaining the same network capacity. All benchmarks labeled as DL-based in the figures of this section represent deep learning-based methods.

A. FMCW FOR SENSING AND OFDM FOR COMMUNICATION

We first focus on the scenario that the communication signals use OFDM waveform while the sensing signals use FMCW waveform. Under this scenario, we study the classification accuracy of the proposed NN model for communication and sensing channels using the confusion matrix, which is seen in Fig. 3. The rows of the confusion matrix correspond to the true class and the columns correspond to the predicted class. The diagonal and off-diagonal cells correspond to correctly and incorrectly classified observations, respectively. For example, the accuracy of correctly and incorrectly detected OFDM channels is 99.0% and 1.0%, respectively. As shown in Fig. 3, an accuracy of around 94% is obtained in all cases. This means that the proposed NN model is suitable for classifying communication signals and sensing signals. Next, we will show how the model performs under various conditions.

Fig. 4 shows the detection rate of communication and sensing signals according to SNR. Our method is superior to the traditional FFT method and original channel method when the SNR is higher than -10 dB. The model can reach a detection rate of more than 95% when the SNR is 0 dB, which shows that our method is robust against noise. The reason for the 50% detection rate of the original channel in Fig. 4 is that it is almost the same in terms of channel magnitude and channel phase as observed in Fig. 2. Also, the distinction between the FFT phase and the Hankelized matrices in Fig. 2 explains why utilizing the FFT phase and singular values of the Hankelized matrix from a partially captured channel enables more effective classification than other methods.

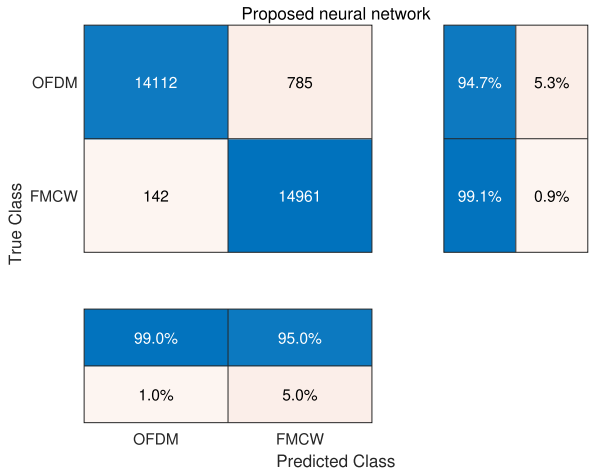

FIGURE 3. Confusion matrix of the proposed NN.

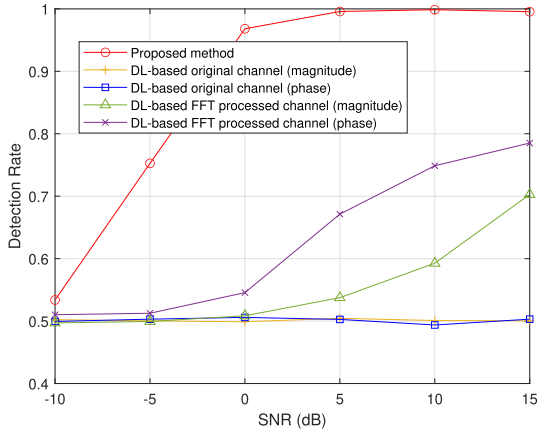

FIGURE 4. Detection rate according to SNR in a scenario where FMCW is used for sensing and OFDM is used for communication.

Notably, the proposed method shows a remarkable performance when the training set size exceeds 1000 in Fig. 5 due to the fact that our proposed method is more effective at leveraging the available data compared to other methods. This shows that the proposed method can still be effective on small amounts of data. This NN framework is minimally affected by the number of training dataset.

Fig. 6 shows the detection rate versus the number of pilot symbols when the SNR is 10 dB. The proposed NN model outperforms benchmarks regardless of the number of pilot symbols. The detection rate of the NN model is more than 90% even when the number of pilot symbols is 8. This implies that the NN model can maintain high detection rates and reliable performance without the need for strict requirements on the pilot symbol configuration or bandwidth allocation.

Fig. 7 shows the detection rate performance according to the variations of SNR at the test phase. For example, if the SNR margin is 5 dB and the NN is trained at 10 dB, then the test of the NN model is conducted within the range of 7.5 dB to 12.5 dB. As seen in Fig. 7, the NN model achieves a detection rate of more than 90% when the SNR margin is

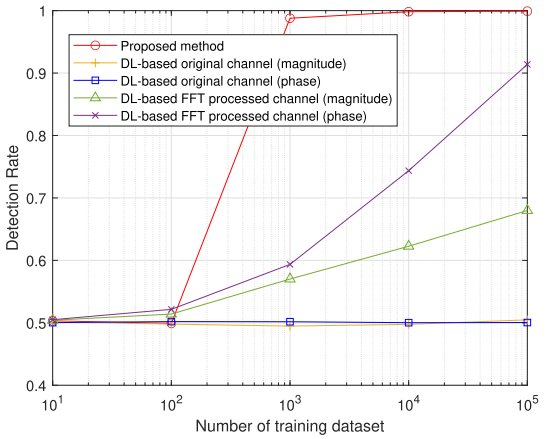

FIGURE 5. Detection rate according to the size of training dataset in a scenario where FMCW is used for sensing and OFDM is used for communication.

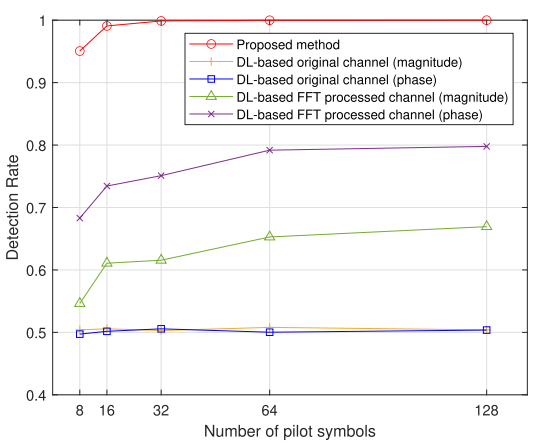

FIGURE 6. Detection rate according to the number of pilot symbols in a scenario where FMCW is used for sensing and OFDM is used for communication.

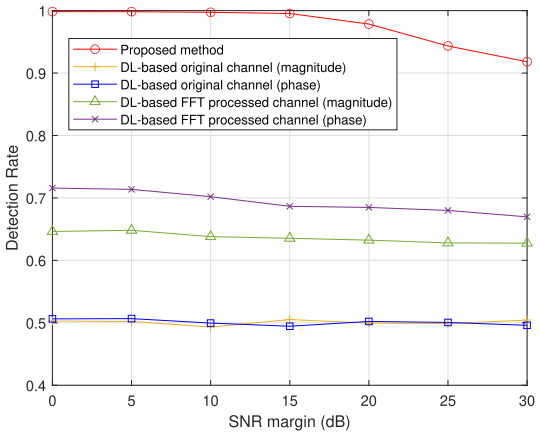

FIGURE 7. Detection rate according to variations of SNR at the test phase in a scenario where FMCW is used for sensing and OFDM is used for communication.

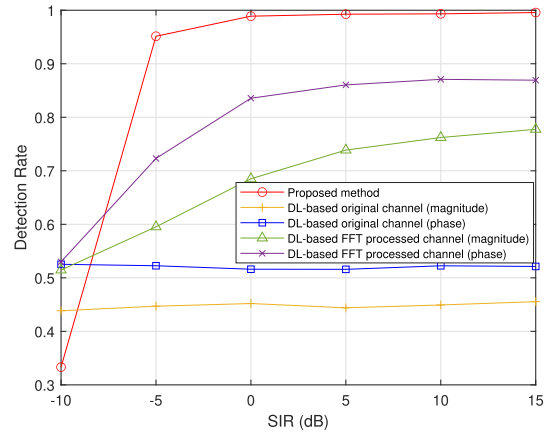

FIGURE 8. Detection rate according to SIR where FMCW is used for sensing and OFDM is used for communication.

less than 30 dB, which indicates that the proposed method performs well in dynamically changing environments during the testing phase. This capability is vital for NN-assisted wireless communication systems.

In Fig. 8, we investigate the detection rate of communication as a function of the SIR, which is defined as the ratio between the received signal strength of the communication signal and the received signal strength of the sensing signals as the interference. It can be seen the detection rate increases with the level of SIR, as a higher SIR means a clearer and stronger communication signal relative to the sensing signal and noise in the environment. Our method performs better than the FFT method and the original channel method when the SIR is higher than -7 dB when the communication waveform is OFDM and the sensing waveform is FMCW. When the SIR is higher than 0 dB, the FFT method can achieve a detection rate slightly higher than 85%. However, the detection rate of our proposed method remains above 90% for SIR values greater than -5 dB.

We investigate the robustness of the proposed NN model with respect to the choice of loss function, as presented in Table 2. Two widely used loss functions—MSE and cross entropy—are considered in the evaluation. We analyze the performance trends under varying conditions of SNR, training dataset size, and the number of pilot symbols. In most cases, two loss function settings shows the similar performances. This consistency indicates that the proposed method exhibits low sensitivity to the selection of the loss function, thereby demonstrating its inherent robustness.

B. OFDM-LFM FOR BOTH COMMUNICATION AND SENSING

In addition, we also investigate the performance of our proposed framework under the scenario that both the communication signal and the sensing signal utilize the OFDM-LFM waveform.

TABLE 2. Detection rate across different loss functions (All values are expressed as the mean ± standard deviation.)

(a) According to SNR (dB)					
NN models ＼ Parameter values	-10	-5	0	5	10
Proposed model w/ MSE	0.5538 ± 0.0054	0.769 ± 0.0034	0.9687 ± 0.0014	0.9940 ± 0.0006	0.9971 ± 0.0006
Proposed model w/ cross entropy	0.5469 ± 0.0041	0.7668 ± 0.0042	0.9720 ± 0.0014	0.9972 ± 0.0005	0.9990 ± 0.0003
(b) According to the size of training dataset					
NN models ＼ Parameter values	10^1	10^2	10^3	10^4	10^5
Proposed model w/ MSE	0.5002 ± 0.0053	0.5031 ± 0.0042	0.9878 ± 0.0004	0.9982 ± 0.0003	0.9999 ± 0.0003
Proposed model w/ cross entropy	0.4987 ± 0.0051	0.5023 ± 0.0047	0.9735 ± 0.0011	0.9989 ± 0.0003	0.9999 ± 0.0002
(c) According to the number of pilot symbols					
NN models ＼ Parameter values	8	16	32	64	128
Proposed model w/ MSE	0.9554 ± 0.0024	0.9854 ± 0.0009	0.9987 ± 0.0003	0.9995 ± 0.0002	0.9999 ± 0.0001
Proposed model w/ cross entropy	0.9487 ± 0.0019	0.9843 ± 0.0012	0.9983 ± 0.0004	0.9997 ± 0.0002	0.9999 ± 0.0001

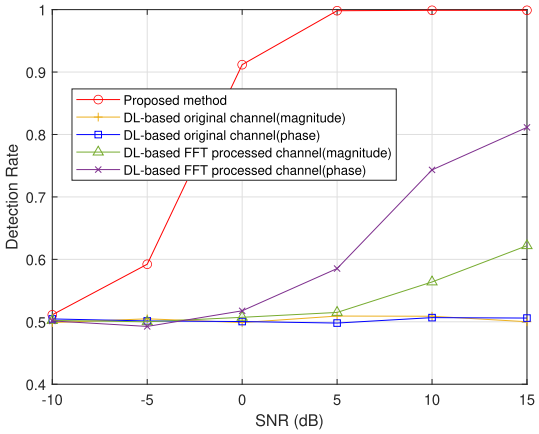

FIGURE 9. Detection rate according to SNR in a scenario where OFDM-LFM is used for both sensing and communication.

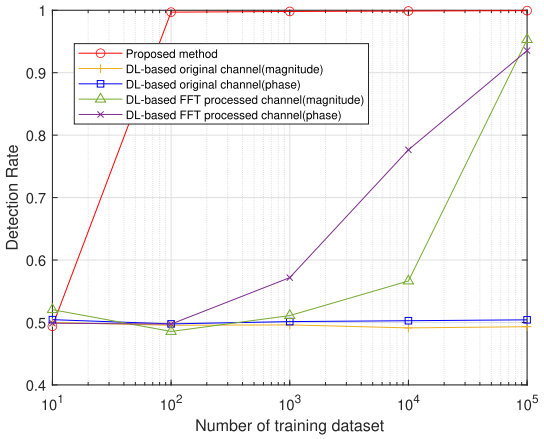

FIGURE 10. Detection rate according to the size of training dataset in a scenario where OFDM-LFM is used for both sensing and communication.

In Fig. 9, we observe that the detection rate of communication and sensing signals as the SNR varies. At -10 dB, the performance is slightly lower than the previous scenario. But our proposed method consistently outperforms traditional FFT and original channel methods when the SNR exceeds -5 dB. This demonstrates our model's superior ability to handle moderate to high noise levels, ensuring more reliable signal classification in such environments.

Fig. 10 highlights that the relationship between the detection rate and the size of the training set. Remarkably, our method maintains excellent performance even when the training set size exceeds 100 samples. This requires less data than previous scenarios. This indicates that the proposed framework is more effective with relatively small datasets, underscoring its practicality and efficiency in scenarios where extensive data collection is not feasible.

Fig. 11 shows that how varying the number of pilot symbols affects our network's performance at an SNR of 10 dB. The findings reveal that our proposed framework consistently outperforms other methods, regardless of the number of pilot symbols used. 99% detection rate is achieved with 16 pilot symbols, indicating our model's efficient utilization of pilot symbols for enhanced signal classification.

The robustness of our method to SNR margins is illustrated in Fig. 12. The NN model achieves a detection rate of over

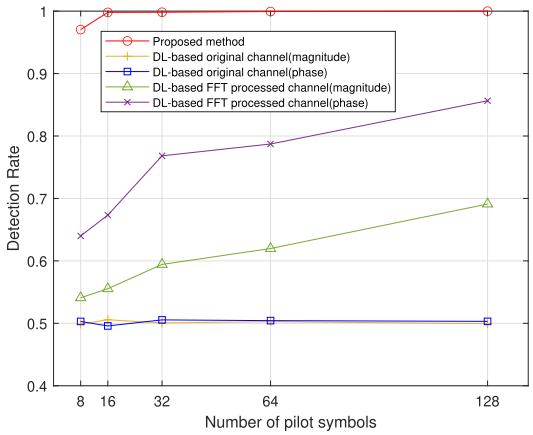

FIGURE 11. Detection rate according to the number of pilot symbols in a scenario where OFDM-LFM is used for both sensing and communication.

80% as long as the SNR variation remains within 30 dB. This demonstrates our method's resilience and consistent performance across a broad range of SNR conditions, ensuring reliable operation in diverse environments.

Fig. 13 shows the detection rate of communication signals as a function of the SIR between the communication and sensing signals. The detection rate increases with

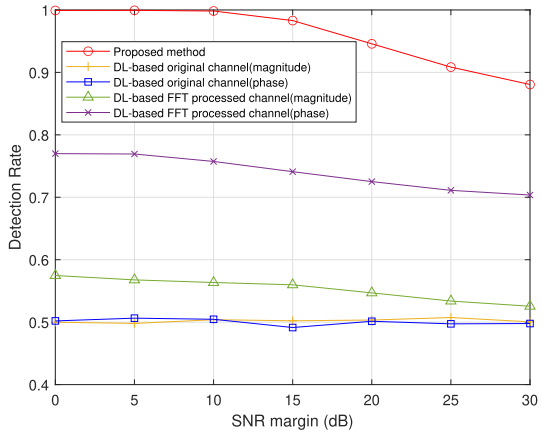

FIGURE 12. Detection rate according to variations of SNR at the test phase in a scenario where OFDM-LFM is used for both sensing and communication.

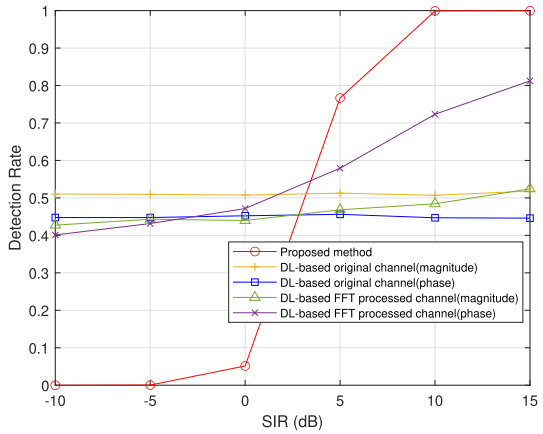

FIGURE 13. Detection rate according to SIR in a scenario where OFDM-LFM is used for both sensing and communication.

the SIR, surpassing 70% when the ratio exceeds 5 dB. This performance is less desirable compared to previous experimental results as seen in Fig. 8, in which OFDM and FMCW are used for communication and sensing signals, respectively. However, it still demonstrates the capability of our model to handle challenging conditions with significant signal overlap, maintaining strong detection accuracy even under these environments.

V. CONCLUSION

In this paper, we propose a new framework for classifying sensing and communication signals using the singular values of the Hankelized matrices of captured channels. Our proposed framework is based on the mathematical property that the Hankelized matrix of an equidistant sampled signal of sparsely superimposed radio waves has a low-rank property. Frequency-modulated signals cannot satisfy this property due to non-arithmetic progression in the phase domain. Therefore, we use the singular values of the Hankelized matrix for classification. Simulation results show that the detection rate of the proposed model has remarkable classification performance based on SNR, the size of training dataset, and the number of pilot symbols. It is important to highlight that the model shows significant potential for applications in ISAC, whether different or identical waveforms such as FMCW, OFDM and OFDM-LFM are used for communication and sensing tasks. In future work, we will extend our study by incorporating real-world data for both training and test. Additionally, more advanced NN architectures, such as transformers, can be explored to further refine model performance. Furthermore, utilizing NN models as feature extractors could enable the discovery of more informative representations beyond those from the singular values of the Hankelized matrix, potentially refining the overall model effectiveness.

REFERENCES

[1] Q. Huang, H. Chen, and Q. Zhang, "Joint design of sensing and communication systems for smart homes," *IEEE Netw.*, vol. 34, no. 6, pp. 191–197, Nov. 2020.

[2] A. Ali, N. Gonzalez-Prelcic, R. W. Heath Jr., and A. Ghosh, "Leveraging sensing at the infrastructure for mmWave communication," *IEEE Commun. Mag.*, vol. 58, no. 7, pp. 84–89, Jul. 2020.

[3] W. Zhou, R. Zhang, G. Chen, and W. Wu, "Integrated sensing and communication waveform design: A survey," *IEEE Open J. Commun. Soc.*, vol. 3, pp. 1930–1949, 2022.

[4] F. Liu, Y. Cui, C. Masouros, J. Xu, T. X. Han, Y. C. Eldar, and S. Buzzi, "Integrated sensing and communications: Toward dual-functional wireless networks for 6G and beyond," *IEEE J. Sel. Areas Commun.*, vol. 40, no. 6, pp. 1728–1767, Jun. 2022.

[5] E. G. Larsson, O. Edfors, F. Tufvesson, and T. L. Marzetta, "Massive MIMO for next generation wireless systems," *IEEE Commun. Mag.*, vol. 52, no. 2, pp. 186–195, Feb. 2014.

[6] R. W. Heath Jr., N. González-Prelcic, S. Rangan, W. Roh, and A. M. Sayeed, "An overview of signal processing techniques for millimeter wave MIMO systems," *IEEE J. Sel. Topics Signal Process.*, vol. 10, no. 3, pp. 436–453, Apr. 2016.

[7] Y. Dong, F. Liu, and Y. Xiong, "Joint receiver design for integrated sensing and communications," *IEEE Commun. Lett.*, vol. 27, no. 7, pp. 1854–1858, Jul. 2023.

[8] Z. Wei, H. Qu, Y. Wang, X. Yuan, H. Wu, Y. Du, K. Han, N. Zhang, and Z. Feng, "Integrated sensing and communication signals towards 5G-A and 6G: A survey," *IEEE Internet Things J.*, vol. 10, no. 13, pp. 11068–11092, Jul. 2023.

[9] D. K. Pin Tan, J. He, Y. Li, A. Bayesteh, Y. Chen, P. Zhu, and W. Tong, "Integrated sensing and communication in 6G: Motivations, use cases, requirements, challenges and future directions," in *Proc. 1st IEEE Int. Online Symp. Joint Commun. Sens. (JC&S)*, Feb. 2021, pp. 1–6.

[10] Z. Wei, W. Jiang, Z. Feng, H. Wu, N. Zhang, K. Han, R. Xu, and P. Zhang, "Integrated sensing and communication enabled multiple base stations cooperative sensing towards 6G," *IEEE Netw.*, vol. 38, no. 4, pp. 207–215, Jul. 2024.

[11] H. Kim, J. Kim, and D. Hong, "Dynamic TDD systems for 5G and beyond: A survey of cross-link interference mitigation," *IEEE Commun. Surveys Tuts.*, vol. 22, no. 4, pp. 2315–2348, 4th Quart., 2020.

[12] Y. Niu, Z. Wei, L. Wang, H. Wu, and Z. Feng, "Interference management for integrated sensing and communication systems: A survey," *IEEE Internet Things J.*, vol. 12, no. 7, pp. 8110–8134, Apr. 2024.

[13] X. Cheng, D. Duan, S. Gao, and L. Yang, "Integrated sensing and communications (ISAC) for vehicular communication networks (VCN)," *IEEE Internet Things J.*, vol. 9, no. 23, pp. 23441–23451, Dec. 2022.

[14] K. B. Cooper, R. J. Dengler, N. Llombart, B. Thomas, G. Chattopadhyay, and P. H. Siegel, "THz imaging radar for standoff personnel screening," *IEEE Trans. THz Sci. Technol.*, vol. 1, no. 1, pp. 169–182, Sep. 2011.

[15] J. G. Andrews, S. Buzzi, W. Choi, S. V. Hanly, A. Lozano, A. C. K. Soong, and J. C. Zhang, "What will 5G be?" *IEEE J. Sel. Areas Commun.*, vol. 32, no. 6, pp. 1065–1082, Jun. 2014.

[16] W.-Q. Wang, "An orthogonal frequency division multiplexing radar waveform with a large time-bandwidth product," *Defence Sci. J.*, vol. 62, no. 6, pp. 427–430, Nov. 2012.
[17] M. Li, W.-Q. Wang, and Z. Zheng, "Communication-embedded OFDM chirp waveform for delay-Doppler radar," *IET Radar, Sonar Navigat.*, vol. 12, no. 3, pp. 353–360, Mar. 2018.
[18] T. Wild, V. Braun, and H. Viswanathan, "Joint design of communication and sensing for beyond 5G and 6G systems," *IEEE Access*, vol. 9, pp. 30845–30857, 2021.
[19] J. A. Zhang, F. Liu, C. Masouros, R. W. Heath Jr., Z. Feng, L. Zheng, and A. Petropulu, "An overview of signal processing techniques for joint communication and radar sensing," *IEEE J. Sel. Topics Signal Process.*, vol. 15, no. 6, pp. 1295–1315, Nov. 2021.
[20] G. Song, M. Jang, and D. Yoon, "CNN-based modulation classification for OFDM signal," in *Proc. Int. Conf. Inf. Commun. Technol. Converg. (ICTC)*, Oct. 2021, pp. 1326–1328.
[21] B. Kim, V. Sathyanarayanan, C. Mecklenbräuker, and P. Gerstoft, "Deep learning-based modulation classification for OFDM systems without symbol-level synchronization," in *Proc. IEEE Int. Conf. Acoust., Speech, Signal Process. Workshops (ICASSPW)*, Jun. 2023, pp. 1–5.
[22] S. An, M. Jang, and D. Yoon, "Classification of Single- and multi-carrier signals using CNN based deep learning," in *Proc. 7th IEEE Int. Conf. Netw. Intell. Digit. Content (IC-NIDC)*, Nov. 2021, pp. 196–199.
[23] W.-H. Lee and M. Kim, "NsigNet: A neural network design for detecting the number of signals under sparse observations," *IEEE Internet Things J.*, vol. 11, no. 11, pp. 19355–19367, Jun. 2024.
[24] J.-H. Kim, D.-H. Kim, M. Ozger, and W.-H. Lee, "An NN-aided near-and-far-field classifier via channel hankelization in XL-MIMO systems," *IEEE Access*, vol. 12, pp. 41934–41941, 2024.
[25] J.-H. Kim, M. Ozger, and W.-H. Lee, "CR2Net: A neural network-based classifier for Rician and Rayleigh channels via hankelization," *IEEE Wireless Commun. Lett.*, vol. 13, no. 5, pp. 1235–1239, May 2024.

LINYI ZHANG received the B.S. degree in information engineering from Shanghai Jiao Tong University, in 2022, and the M.S. degree in machine learning from the KTH Royal Institute of Technology, in 2024. His primary research interests include signal processing and machine learning in wireless communication.

MUSTAFA OZGER received the B.Sc. degree in electrical and electronics engineering from Middle East Technical University, Ankara, Tükiye, in 2011, and the M.Sc. and Ph.D. degrees in electrical and electronics engineering from Koç University, Istanbul, Tükiye, in 2013 and 2017, respectively. He is currently a Researcher with the KTH Royal Institute of Technology, Stockholm, Sweden, and an Assistant Professor with Aalborg University, Copenhagen, Denmark. His research interests focus on aerial and vehicular networks as well as the Internet of Things.

WOONG-HEE LEE (Member, IEEE) received the B.S. degree in electrical engineering from Korea Advanced Institute of Science and Technology (KAIST), Daejeon, South Korea, in 2009, and the Ph.D. degree in electrical engineering from Seoul National University, Seoul, Republic of Korea, in 2017. From 2017 to 2019, he was an Experienced Researcher with Advanced Standard Research and Development Laboratories, LG Electronics Inc., Seoul. From 2019 to 2020, he was a Postdoctoral Researcher with the Department of Communication Systems, KTH Royal Institute of Technology, Stockholm, Sweden. From 2020 to 2021, he was an Experienced Researcher with Ericsson Research, Stockholm. From 2021 to 2024, he was an Assistant Professor with the Department of Control and Instrumentation Engineering, Korea University, Sejong-si, Republic of Korea. Since March 2024, he has been an Assistant Professor with the Division of Electronics and Electrical Engineering, Dongguk University, Seoul. His research interests include signal processing, machine learning, and game theory in wireless communications.